University of Baghdad
College of Engineering
JOURNAL OF ENGINEERING

Journal of Engineering
journal homepage: www.jcoeng.edu.iq
Volume 31 Number 6 June 2025

Improvement of the Nonparallel Helical Gear Drive Performance Using the Modified Asymmetric Teeth with Tip Relief

Mohammed Abdulaal Kadhim *, Mohammad Qasim Abdulah

Department of Mechanical Engineering, College of Engineering, University of Baghdad, Baghdad, Iraq

ABSTRACT

Overheating is a common issue in a nonparallel helical gearing system. The reason is the high friction, sliding velocity, and tangential force that occurs between meshed gear teeth. These factors can result in negative outcomes such as increased power loss, low gear efficiency, breakdown, and scuffing. Two types of non-parallel helical gears have been utilized to estimate the meshing heat fluxes of a pair of non-parallel gear systems. The scenario involves a design of standard helical teeth and a modified asymmetric non-parallel helical system. The asymmetric tool designe serves as a reference for preparing a modified asymmetric helical gear, which the CNC machine can then cut. The hybrid curve has been compounded from three parts (hypocycloid-involute-tip relief) on the loaded side and (hypocycloid-involute-epicycloid) on the unloaded side, using different pressure angles for each side. The non-parallel helical gear drive that has teeth modified asymmetrically is better than a standard non-parallel helical gear drive. The numerical results indicate the best enhancements in the maximum contact stress and tooth root stress percentages are about 12.253% and 8.91%, respectively. Adjusting the helical gear teeth surface improves the generated heat flux, resulting in an enhancement percentage of approximately 39.567%. The enhancement percentage of pitch deviation under different rotational speeds has been the best compared with the standard case under the same conditions and a high-speed range with high local temperatures reaching about 15% and is good at the low-speed range by 10%.

Keywords: Modified asymmetric helical teeth, Tip relief modification, Coefficient tooth friction, Contact stress, Heat friction generated.

1. INTRODUCTION

Non-parallel gears are mechanical drives utilized in numerous power transmission applications, encompassing cars, industrial machinery, airplanes, and marine equipment

*Corresponding author
Peer review under the responsibility of University of Baghdad.
https://doi.org/10.31026/j.eng.2025.06.12

Article received: 23/11/2024
Article revised: 25/01/2025
Article accepted: 04/02/2025
Article published: 01/06/2025

(Litvin et al., 2007). Recommended are lightweight gears that exhibit exceptional reliability for many industrial requirements. To enhance gearbox improvements, the gear is advised based on its high load capacity, durability, low cost, and high speeds **(Colbourne, 2012)**. A fundamental characteristic of helical gears is that the axes of the gears do not need to be parallel. This situation arises when the pitch helix angle is aligned in the same direction. This gear design is known as non-parallel-axes helical gears **(Jelaska, 2012)** and is conjugated at an intersection angle between gear axes which will be between $\lambda > 0^{\circ}$ and $\lambda \leq 90^{\circ}$. **(Norgauer et al., 2017)**. Nonparallel-axes helical gears are used in applications necessitating a high gear ratio under limited spatial conditions. These devices provide power transmission between shafts that are neither parallel nor intersecting **(Trubachev et al., 2018)**. The contact region between the surfaces of the paired crossed-tooth gears indicates a notable elastic point contact. A common issue associated with a nonparallel-axes gearing system is the occurrence of overheating. The heating source in the engagement of gear teeth can be attributed to the significant factors of high friction, sliding velocity, and tangential force. Friction arises between the tooth profiles during the engagement process. The identified reasons result in negative outcomes, including heightened power loss, diminished gear efficiency, potential breakdowns, and scuffing **(Wang et al., 2017)**. The high sliding speed and surface pressure are caused by tooth surface scoring and a lack of lubrication. This causes unnecessary frictional heat and severe overheating of the meshing teeth. Scoring is a phenomenon that happens quickly in areas with high temperatures, resulting in a higher rate of wear. The approaches utilized to avoid the scoring region include choosing proper parameters and the flow of lubricant **(Armenakas, 2016)**. Helical gear geometry modifications involve changing the involute profile or adjusting the gear lead angle. The numerical and experimental methodologies help to overcome the common impediments and challenges in determining the true causes of this occurrence. The ellipse shape of contact that causes wear was estimated by using simulation tools. The simulation is influenced by linear static stress and volumetric wear, which arise from several key factors, involving the coefficient of tooth friction, tangential force, and sliding velocity model **(Pakhaliuk and Poliakov, 2018)**.

Despite large investigations in the gears field, researchers remain concerned regarding the performance of non-parallel helical gear drives. Analyzed the crossed helical gear drive mathematically. Utilizing the ANSYS software program. the stress analysis of the innovative crossing helical gear is carried out. The FEA results are shown utilizing a 10° shaft angle in conjunction with MATLAB-created three-dimensional solid models of a crossed helical gear pair. The results show that the pinion can withstand a maximum von Mises stress of 793.69 MPa. The innovative gear pair has better contact strength and capacity, as shown by reduced contact stress values compared to the crossed-axis involute gear drive. **(Liang, 2021**) established a parallel rack profile using a fourth-order polynomial. The design enhanced flank geometries and examined their characteristics. The deformation and load distribution in different engagements were reviewed according to the dominant load and plastic material stiffness. The geometries of the two wheels are obtained by meshing each wheel with one side of the rack, allowing both wheels to intermesh while accounting for shaft angles that deviate from 90°. Innovative flank shapes and changes for crossed helical gears are being devised to enhance their efficiency. **(Becker et al., 2022)** studied the technical difficulties and service landscape of high-strength gears. Analyzed the technical challenges associated with design, and manufacturing integration. The focus is on the development direction of high-strength gears. The article delves into the latest findings in anti-fatigue design,

manufacture, and service performance assessment of high-strength gears. The objective is to encourage the development and use of high-strength gear technology. **(Wu et al., 2024)** studied mathematically generation standard and non-standard spur gear involute teeth. Investigated the bending stress in the root fillet and stress concentration reduction in the teeth gear surface. The utilization of non-standard gear teeth boosts bending strength by approximately 33% and reduces contact stress by roughly 20%. **(Alex, 2009)** investigated contact stress in standard spur gears analytically and numerically affected by different geometrical design parameters. Regarding contact stress, four different cases (involute, cycloidal, epicycloidal, and hypocycloidal) have been compared. Results show that compared with involute teeth, reduction in contact stress for the same design is 30% for cycloid, 46% for epicycloidal, and 21% for hypocycloidal. Generally, in various mechanical applications, gears transfer motion and power between shafts at any skew angle **(Farhangdoost, 2010)**. The simulation of CFD has been used as an effective tool for achieving accuracy. Proposing the implementation of oil-lubricated distribution within the gearbox system and the application of airflow management. **(Miltenović and Banić, 2020)** developed a methodological model for estimating the time-dependent behavior of the thermo-fluid case. This method was presented for a gearbox unit comprising three interlocking gears. **(Yazdani, 2015)** examined friction generation and assessed the transient thermal properties of spiral bevel gears. He employed numerical simulation as a method to investigate the friction heat on an actual tooth geometry under realistic actuating conditions. The objective was to analyze the friction heat generation during the meshing of a spiral bevel gear. Establishing a correlation between the results of the Finite Element method, types of damage, and the efficiency of gears. **(Wang, 2017)** proposed a fast procedure for predicting the gearbox system temperature using the Finite Element Analysis. The gearbox is designed to take the calculations of the ambient temperatures of the gear unit to define the thermal stability. This process was presented to allow the gear system designers to use the fast FEA calculations for temperature. **(Miltenović and Banić, 2020)** presented a theoretical and numerical investigation of mesh gear efficiency, one-tooth friction coefficient, and wear crossed helical teeth especially that made of Fe1.5Cr0.2Mo sintered steel with sinter hardening treatment. The method gives the determinations of the wear load capacity of the worm with a helical gear. The results showed the product developed by the important clues for indicators for calculating the worm with a helical gear. The treated sintered steel has about a 20% smaller friction coefficient and gives a higher mesh efficiency of about 6% compared with those gears that haven't had any additional treatment **(Miltenović, 2015)**.
Previous investigations have revealed gearing patterns to improve mechanical performance. They presented enhancement load-carrying gear designs utilizing traditional research and experience. Gear designers use non-standard tooth forms to improve peak geometry and mechanical strength. This study presents the manufacturing of a non-conventional gear tooth profile. They will be assembled with a test-gear rig. Two types of non-parallel helical gears have been employed to assess the meshing heat fluxes associated with a pair of non-parallel gears. The system consists of standard non-parallel helical symmetric teeth featuring 7 normal modules, 20 normal pressure angles, and 22.5 helix angles. A non-parallel helical system has been modified to feature an asymmetric tooth profile for both the left and right sides. The unloaded side, comprises compounded teeth featuring Epicycloidal, Involute, and Hypocycloidal components, with specifications of 7 modules, a 25-degree pressure angle, and a 9 mm rolling circle. The loaded side features an Involute-Hypocycloidal profile with a linear intermediate tip relief modification. This configuration includes 7

modules, a pressure angle of 14.5 degrees, a rolling circle diameter of 9 mm, and an optimized tip relief design.
The manufacturing process is executed using computer numerical control (CNC) machines. The simulation of the optimal tool is performed using the SOLIDWORKS software package, which is utilized to generate these helical gear cases **(Kurowski, 2016)**.

2. CREATION OF INVOLUTE AND NON-INVOLUTE GEAR TEETH.

The standard and non-standard gear tooth profiles can be created by a similar generation method by using the gear cutting **(Babichev, 2017)**. The novelty of this methodology is that it creates a non-conventional tooth surface that is represented realistically. The resulting curve is not an involute arc such as shown in several research but is a hybrid of groups from curves that can't be created by the classical known method.

2.1 Involute Gear Tooth.

In general, the gear tooth fillet region is typically characterized by a trochoid curve; however, this aspect has often been overlooked by many researchers. This method facilitates the maintenance of creative optimization accuracy. The Creation method is outlined as shown: **(Guilbault, 2006; Babichev and Storchak, 2018)**.

- The rack cutter tool is defined as the pattern of the tool that will be creating the gear tooth profile. Here, the pitch point of the tool is rigid at the original point. The tool is divided by the pitch line *LL* into two parts having different lengths as shown in **Fig. 1.** The basic tool with the optimum gears conforms according to the standard criteria. **Fig. 2** illustrates the tool's pitch line, divided into equal parts on both sides about the vertical line vv parallel to the vertical centerline.

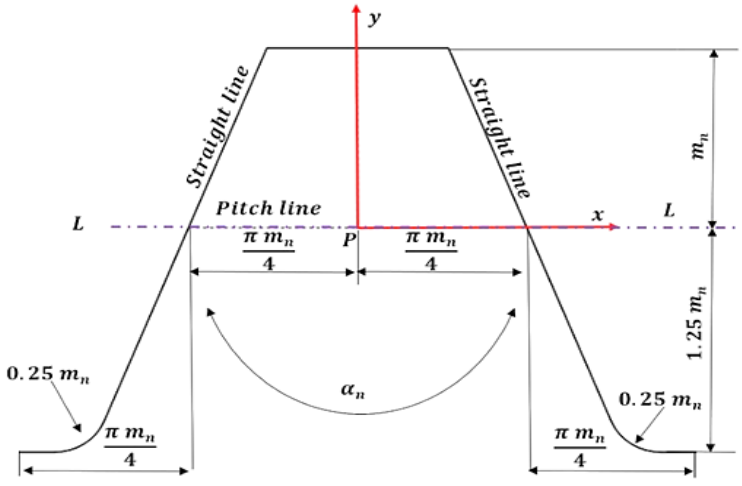

Figure1. The standard tool designation.

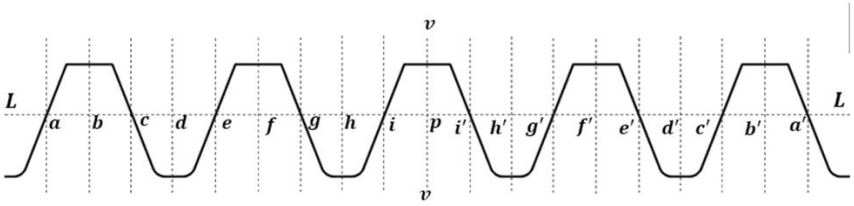

Figure 2. The reference pitch line of the tool.

- The pitch circle of the gear is drawn at the fixed point *O*. It will be divided at equal intervals at shown in **Fig. 3**. The lines are drawn to facilitate correcting alignment by thin lines drawn through these points.

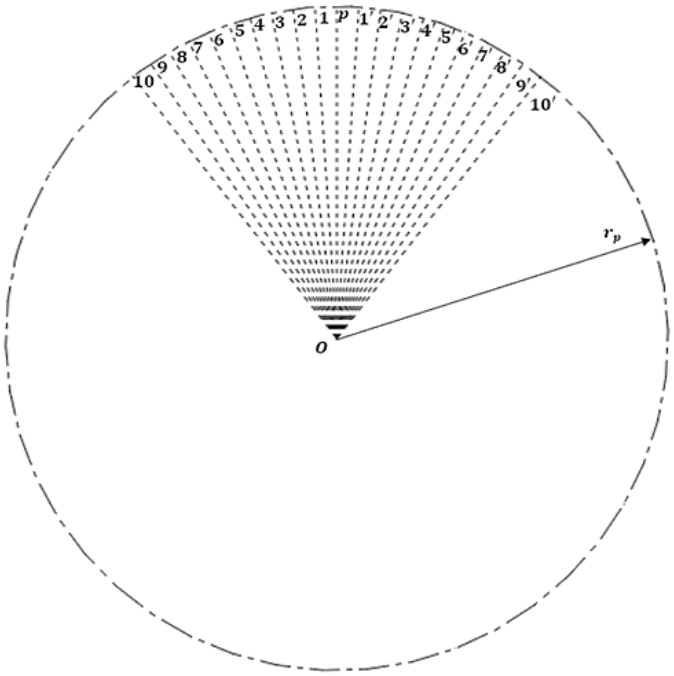

Figure 3. The gear's pitch circle.

- Place the tool reference over the track as in **Fig. 4** which illustrates the pitch line *LL* for the tool should be tangent to the pitch circle of the gear at the intersection point called the pitch point *P*.

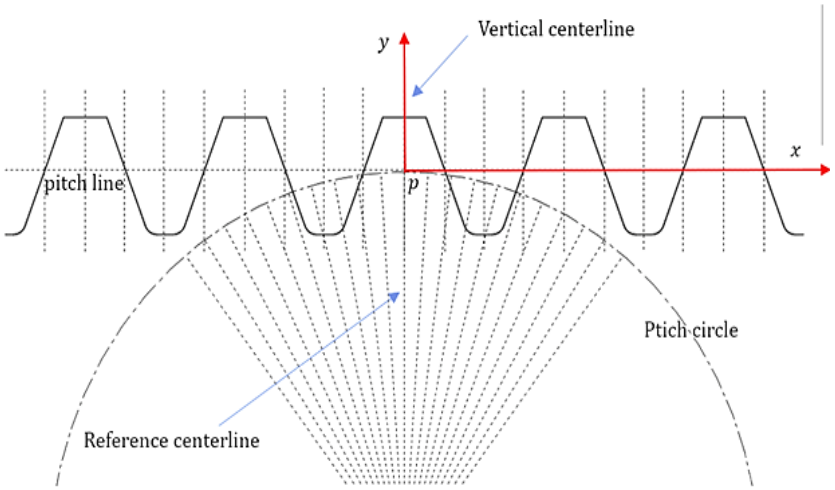

Figure 4. The coordinate system of the pitch circle with respect to the pitch point.

- The resulting points of the tool and the fixing points of the pitch circle coincide. These intervals for the tool indicate the pitch line of the tool is rolled on the pitch circle. This process generates the final tooth form. **Fig. 5** shows the steps of generation of involute toothing.

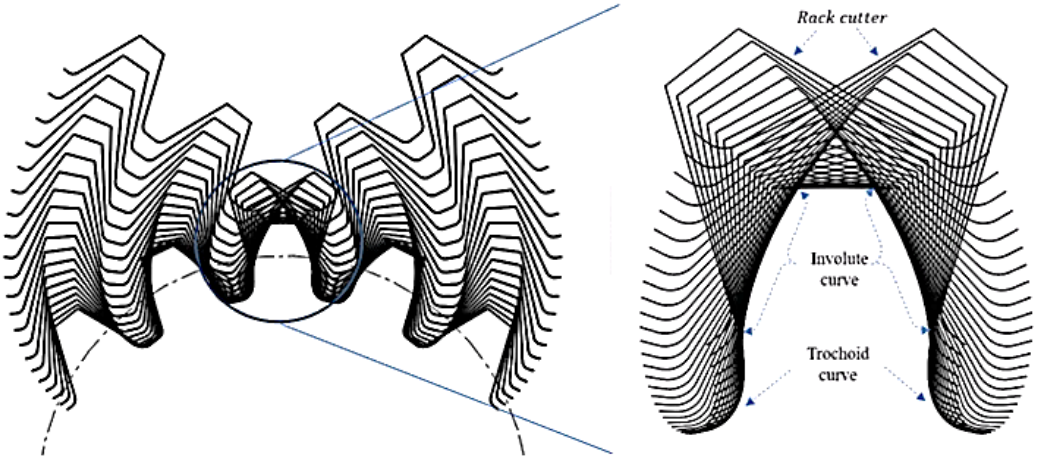

Figure 5. The complete creation of gear.

- In the generation process, the pitch line of the tool would be shifted by a constant amount e away from the pitch cylinder **(Juvinall and Marshek, 2020)**. Therefore, the following condition is to avoid gear tooth undercutting:

$$m_n - e \leq r_p sin\alpha_n{}^2 \quad (1)$$

$$m_n(1 - \frac{e}{m_n}) \leq r_p sin\alpha_n{}^2 \quad (2)$$

In the helical involute teeth, the non-undercutting is validated by defining the quantities:

$$m_t = \frac{m_n}{cos\beta_p} \quad (3)$$

$$\alpha_t = tan^{-1}(\frac{tan\alpha_n}{cos\beta_p}) \quad (4)$$

Hence, the Eq. (3) is becoming

$$m_t(1 - \frac{e}{m_t}) \leq r_p sin^2\alpha_t \quad (5)$$

Or

$$\frac{e}{m_n} \geq 1 - \frac{Z}{2} \times \frac{sin^2\alpha_t}{cos\beta_p} \quad (6)$$

$$\frac{e}{m_n} \geq 1 - \frac{Z(tan^2\alpha_n)}{cos\beta_p(cos^2\beta_p + tan^2\alpha_n)} \quad (7)$$

In the case of $e = 0$, no addendum modification. The minimum number for helical gearing teeth would be

$$Z \geq \frac{2cos\beta_p(cos^2\beta_p + tan^2\alpha_n)}{tan^2\alpha_n} \quad (8)$$

Table. 1 shows the minimum number of helical gear teeth that prevent tooth undercutting occurrence. The optimum minimum number of teeth that will used in this work to avoid undercutting is equal to 14 teeth adopted with 20 normal pressure angles and 22.5 helix angles.

Table 1. Minimum number of helical gear teeth dependent on β_p, and α_n.

Pressure angle α_n	Helix angle in deg β_p					
	0°	15°	22.5°	30°	37.5°	45°
14.5°	32	29	26	22	17	12
20°	18	16	14	12	10	7
25°	12	11	10	8	7	5

2.2 Non-Conventional Tooth Profile.

The modified asymmetric tool consists of two sides. the unloaded high-pressure angle side with a compound curve. The loaded Low-pressure angle side with a compound curve and addendum optimum tip relief modifications. The coordinate $(x_{r^R}, y_{r^R}, \overrightarrow{n_{r^R}})$ and $(x_{r^L}, y_{r^L}, \overrightarrow{n_{r^L}})$ defines the right tool side and the left tool side, respectively. Two points (x_{c^R}, y_{c^R}) and (x_{c^L}, y_{c^L}) **(Abdulaal and Abdulah, 2024)** are applied to determine the cycloid curve's started position for both tool's sides according to the involute function **(Abdullah, 2003)** and straight-line slope **(Seyama et al., 2009)**. **Fig. 6** shows the left and right tool sides with illustrations indications.

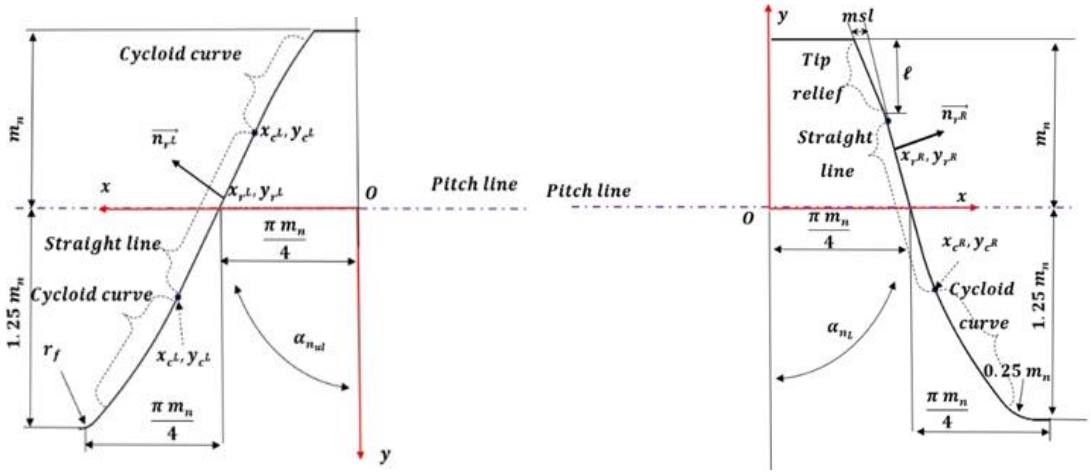

Figure 6. The coordinates system of the modified asymmetric (cycloid-straight line with tip relief) tool.

The same previous approach has been followed to create the asymmetric gear teeth profile but this procedure would be employed twice, once for the right side and then for the left side as shown in **Fig. 7.** After following steps 4 and 5 the procedures are completed for creating a compounded tooth shape as shown in **Fig. 8**.

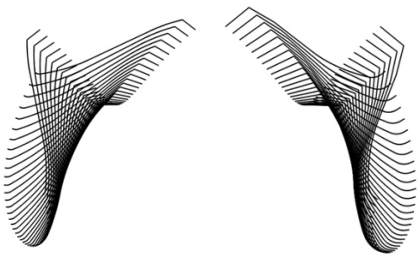

(a) (b)

Figure 7. Left and right tooth shape (a). Epi involute Hypocycloid profile $\alpha_n = 25^\circ$, $R = 9mm$. (b) Involute Hypocycloid profile with tip relief $msl = 60mm$, $\alpha_n = 14.5^\circ$, and $R = 9mm$.

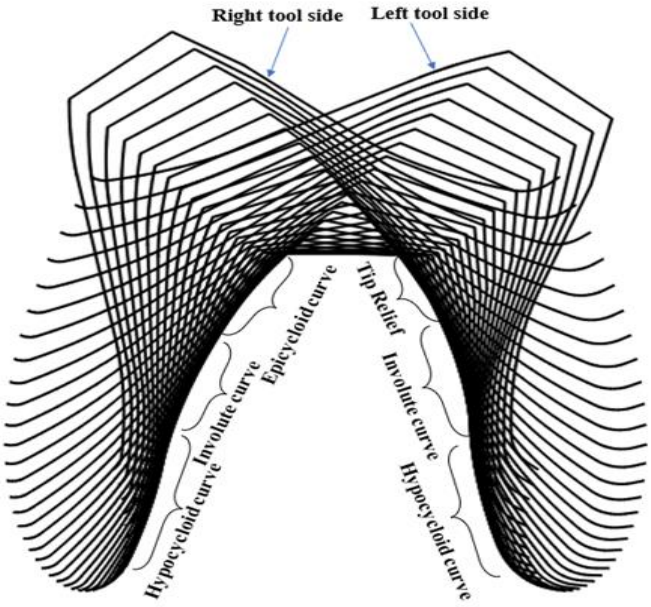

Figure 8. Modified asymmetric tooth profile with tip relief.

In tip relief design, the pitch circle of the gear is considered an important factor in determining the starting point of tip relief. The position of tip relief on the gear tooth surface will be modified according to the pitch radius r_p and the addendum radius r_a of the gear tooth profile as follows **(Temirkhan, 2022)**:

$$\ell = r_a - r_p \tag{9}$$

$$r_\ell = \sqrt{{r_p}^2 - {r_b}^2} \tag{10}$$

$$\varphi_\epsilon = \sqrt{\frac{{r_p}^2}{{r_b}^2} - 1} \tag{11}$$

Where ℓ is the datum length for tip relief, r_ℓ is the rolling length, and φ_ϵ is the rolling angle. The relation between the rolling length and the corresponding rolling angle is illustrated in **Fig. 9**.

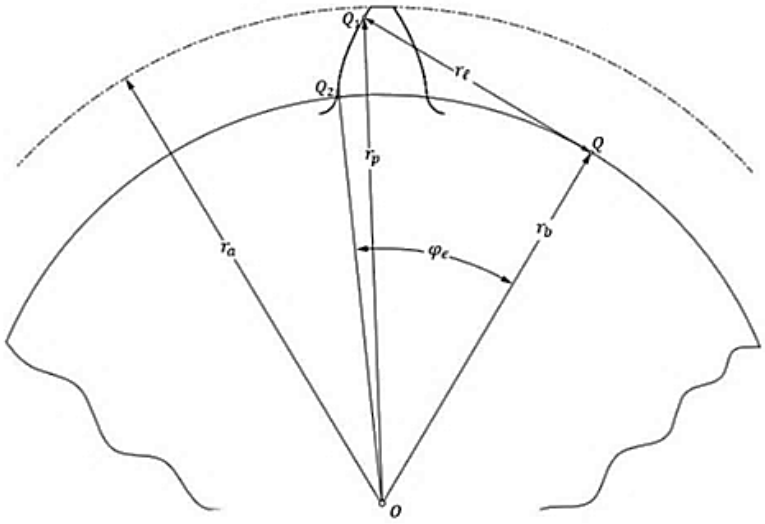

Figure 9. The relation between the rolling length and the corresponding rolling angle.

The values of the amount of tip relief msl and length ℓ of relief can be varied according to the elastic tooth deflection is based on the design parameters such as the tangential applied load, base pitch, and base helix angle specified by tooth geometry, the amount of misalignments and deflections, and tooth stiffness **(Smith, 2003)**. By determining the manufacturing error. The msl value are $60\mu m$ and ℓ adopt at 105.097mm was chosen in this work.

3. HEAT FRICTION GENERATED ANALYSIS.

Friction loss by heat generation and scuffing failure are considered a primary aim to investigate. The significant increase in local temperature led to gear teeth surface failures such as micro-pitting, scoring, and scuffing. It is a contact temperature that occurs on the tooth flank surface at the instant of contact and increases during the meshing. The temperature's value and location on the gear tooth surface are indications of surface tooth failure **(Rackov, 2018).** The implemented profile modifications are one of the worthwhile actions that can be taken to reduce its risk. The tooth geometry parameters with the operating conditions of the gear case are specified. Two points on the surface tooth located before and after the pitch point are the low point single tooth contact LPSTC and the high point single tooth contact HPSTC as shown in the **Fig. 10.** They represent the length of the profile Contact. The generated friction between them on this length is caused by that and reduced by the control of contact. Tip relief modification will reduce the impact shock of the contact at the instant of the engagement starting. An involute surface has been modified to be shorter than that in a standard surface. The hypocycloid surface will involve a high contact ratio due to conformal geometry **(Radzevich and Storchak, 2022; Luo and Jingyu, 2024)**.

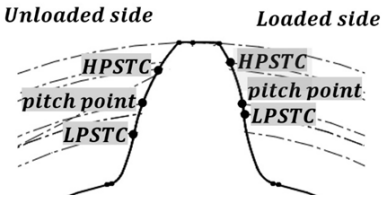

Figure 10. Specific asymmetric tooth position points.

The heat flux resulting between the meshed gear teeth is determined by three critical parameters: the frictional coefficient, the applied normal contact load, and the sliding velocity between the meshed tooth surfaces during engagement, as depicted on the common tangent line of the helical curve in **Fig. 11. (Rattan, 2014).**

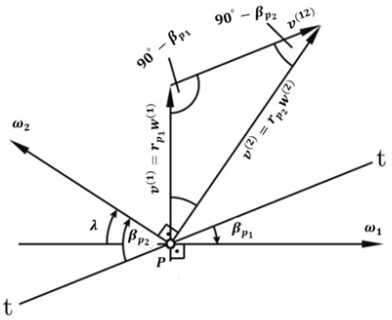

Figure 11. Polygon of sliding velocity.

The Figure shows that under an intersecting angle of the gear axis, it maintains a tangent relationship with the pitch cylinders for the gears that are not parallel to one another. To calculate the sliding velocity, the cosine law is employed as follows **(Vijayaraghavan and Vishnupriyan, 2009)**:

$$v^{(12)} = \left|v^{(2)} - v^{(1)}\right| = w^{(1)} r_{p_1} \sqrt{1 + (\frac{w^{(2)} r_{p_2}}{w^{(1)} r_{p_1}})^2 - 2\frac{w^{(2)} r_{p_2}}{w^{(1)} r_{p_1}} cos\,(\lambda)} \quad (12)$$

Usually, in a non-parallel helical gear drive case the contacting load between meshed gear teeth is accompanied by an axial load due to the effecting of the helix angle as shown in **Fig. 12.** The contact load can be determined normally by it being resolved into three components tangential, radial, and axial or (thrust) parallel with the axis of the shaft as follows

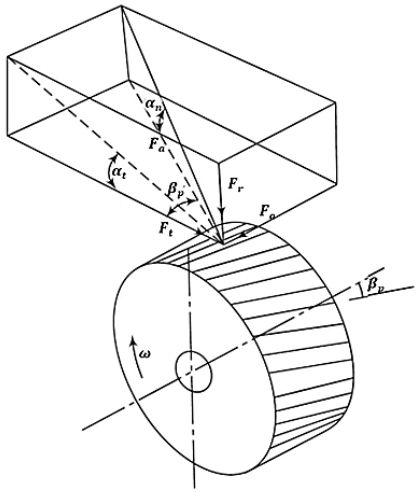

Figure 12. The components of the contact force.

$$F_n = \frac{F_t}{\cos(\alpha_t)\cos\,(\beta_p)} \quad (13)$$

$$F_t = \frac{Power}{v_p} \quad (14)$$

$$F_r = F_t \tan\,(\alpha_t) \quad (15)$$

$$F_a = F_t \tan\,(\beta_p) \quad (16)$$

The frictional heat Q produced between the nonparallel teeth is calculated as follows:

$$Q = \mu\, F_n\, v^{12} \quad (17)$$

In this work, the contact stress analysis has been carried out after the denser mesh is chosen around the area of the pitch point **(Alemu, 2007)** for the gears model which is estimated that have the maximum local temperature. **Fig. 13** shows the 3D mesh of the model volume generated by the ANSYS program **(Stolarski et al., 2018)**. The model has been prepared to satisfy the boundary conditions. The mesh size of the gear tooth element has been gradually refined by increasing mesh density. the material used was Aluminum 7075 which has the properties of are Young Modulus is $7.2e^{+10}\ N/m^2$ and poison's ratio of 0.33. The gear circumstances include a functional power transmission of 20 kW at 1440 rpm at a certain teeth friction coefficient. The friction coefficient may range from around 0.05 to 0.25,

contingent upon the environmental conditions. This study used a 0.15 coefficient value to assess the performance of gears.

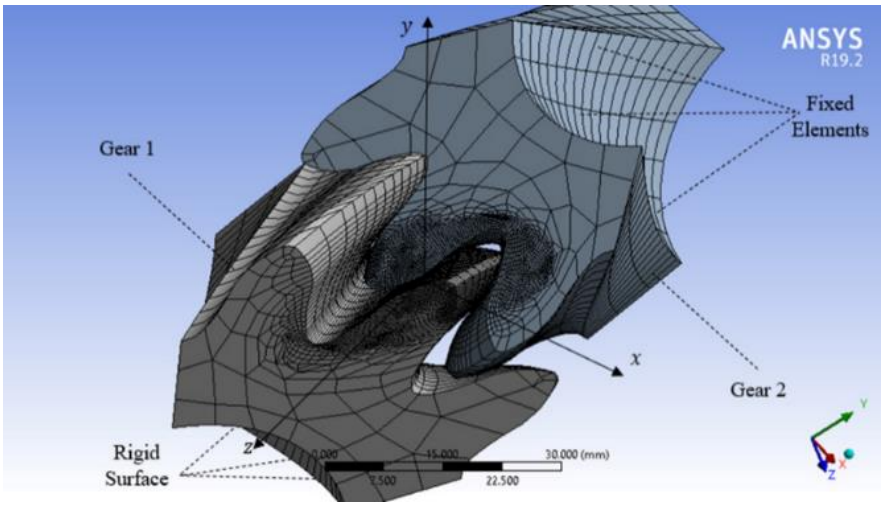

Figure 13. 3D nonparallel helical gear teeth mesh model.

The thermal expansion α changes the operating pitch diameter $D_p$during the work. This change rapidly increases with increased temperature T under the time-varying heat flux fluctuations can be defined as the average of the operating pitch cylinder ΔD_p. The temperature of reference T_{ref} is the ambient temperature during actual work. Any elastic strain that occurs in the gear body changes its pitch cylinder leading to a single normal pitch deviation $S_p$with time both gears indicate an unequal strain. The pitch deviation resulting from thermal expansion can be defined as follows:

$$\Delta D_{p_1} = D_{p_1} \alpha \, (T_1 - T_{ref}) \tag{18}$$

$$\Delta D_{p_2} = D_{p_2} \alpha \, (T_2 - T_{ref}) \tag{19}$$

$$S_p = \Delta D_{p_1} - \Delta D_{p_2} \tag{20}$$

4. EXPERIMENTAL WORKS

This study demands to design and manufacture of the standard and modified nonparallel helical gears drive. Design and assembly of the gear test rig to inspect the cases desired. The CNC machines work to develop the gear teeth surfaces by applying a new topology of tooth profiles. It is achieved by ensuring the relations between the motions of the cutter tool and the wheel blank **(Gosselin, 2018)**. The different helical gear teeth models which are created by computer-aided became ready to manufacture. The dimensions of non-parallel helical gears are listed in **Table 2**.

The milling machine method is used to get the gears due to the special tooth profile. The motion of the machine tool end milling cutter could be obtained according to the program which is provided to CNC. The matching code is controlled by the milling cutter and workbench motions. The gear material used for manufacturing is Aluminum alloy 7075-T6. The mechanical properties and the chemical composition were checked and are detailed in **Tables 3** and **4** respectively.

Table 2. Non-parallel helical gear design parameters.

Gear Parameters	Standard crossed helical symmetric teeth system RD	modified nonparallel helical asymmetric teeth system RD
α_{n_l} deg	20°	14.5°
α_{n_u} deg	20°	25°
β_p deg	22.5°	22.5°
λ deg	45°	45°
Z	14	14
m_n mm	7	7
R mm	---	9
h_a mm	7	7
h_d mm	8.75	8.75
r_p mm	53.04	53.04
$msl\ \mu m$	---	60
ℓ mm	---	3.16

Table 3. The mechanical properties.

Inspection type	Results			
	1	**2**	**3**	**Average**
Environment conditions **°C**	25			
Sample diameter **mm**	25.06	25.19	25.14	/
Tensile resistance **MPa**	572	569	564	568
yield resistance **MPa**	531	527	519	526
Elongations **mm**	8.5	12	11	10.5

Table 4. The chemical composition.

Chemical Elements	Result	Chemical Elements		Result
Si%	0.0390	Ti%		0.0142
Fe%	0.142	Ga%		0.0
Cu%	1.30	V%		0.0
Mn%	0.0420	Zr+Ti		0.0261
Mg%	2.51	Others%	Each	0.0119
Cr%	0.201		Total	0.0
Ni%	0.0	Residual%		Aluminum
Zn%	5.56			

The end milling cutter is fast moved with the other feeding functions coincident with the working axis rotating with the workbench. The helical gear pair could be ready to manufacture. **Figs. 14** and **15** illustrate the vertical CNC machine and manufactured gears, respectively. The nonparallel axes gear test rig is assembled to satisfy the gear cases. The mechanical brake system is designed to generate different braking torques. All test parts are designed and assembled as shown in **Fig. 16** which demonstrates the gear test rig parts.

Figure 14. the vertical CNC machine.

(a) **(b)**

Figure 15. manufactured gears, **(a)** standard non-parallel helical gears, and **(b)** asymmetric non-parallel helical gears.

Figure 16. The non-parallel gear axis test-rig parts.

The critical parameter to specify is the center distance c between two nonparallel helical gear drives fitted in the test gear, which may be verified based on the following:

$$c = r_{p_1} + r_{p_2} = \frac{1}{2}\left(\frac{m_n Z_1}{cos\beta_{p_1}} + \frac{m_n Z_2}{cos\beta_{p_2}}\right) \quad (21)$$

The experience data are recorded under different rotational speeds of about 100-2500 rpm which is done by an increment of 100 rpm controlled by the inverter component. Four external masses (25Kg,50Kg,75 Kg,100 Kg) are applied to generate four different resistance torques. They work directly with meshed gear rotation. The successful execution of non-parallel helical gears functions during operational life when their wear removal value mustn't exceed the limited value for the surface failure. In this experimental case with an increase in the local tooth surface temperature due to the meshing contact, the continuous loss of material is increased during the operating test. Two measurement instruments are used to control and monitor the gears system. Smart Thermal Camera illustrated in **Fig. 17-a** predicts heat generation in the non-parallel helical gears transmission by determining the maximum local temperature at the instant of teeth contact. It is a professional thermal camera module for smartphones that is compact, portable, and easy to operate by connecting with the mobile phone. The base model is 120×90 iR resolution and $-20^{\circ}C \sim 400^{\circ}C$ temperature range. This procedure is fast for the gear's thermal stability inspection and it meeting the requirements of the crossed-gear test setup through out automated alert and monitoring for elevated and reduced temperatures. Normally, cannot be predicted the maximum temperature position on the helical tooth surface an instantaneous because the temperature at any point on the surface tooth will change caused to the heat friction between non-parallel helical teeth. Therefore, the thermal camera position has been adjusted to choose the best perfect reading, and the distance between the temperature emitted from the meshed crossed teeth and the camera sensor is 130mm. A Digital Tachometer illustrated in **Fig. 17-b** calculates the number of operational life speeds for a non-parallel helical gear drive by calculating the number of reflections of reflective tape on the gear shaft.

(a) **(b)**

Figure 17. The Instruments of Gear Test: **(a)** Smart Thermal Camera; **(b)** Digital Tachometer.

5. RESULTS AND DISCUSSION

This section presents the results derived from the examination of the performance of standard teeth in comparison to asymmetric teeth for non-parallel helical gears, followed by a discussion of these findings. Results are presented in three categories analytical, numerical, and experimental. The analytical and numerical methods involve calculating the specific sliding velocities at different rotation angles, evaluating the maximum contact stress, and determining the heat flux resulting between skewed helical teeth.

The results of the sliding velocity for the two cases can be shown in **Fig. 18** which demonstrates the comparison between the effect of the modified tooth geometry on the sliding velocity. The maximum magnitude of velocity appears near the contact points at certain angular positions. Generally, it will be before and after the pitch point. The precise alterations will decrease the sliding distance, thus lowering the velocity at the moment of contact by the implementation of tip relief modification.

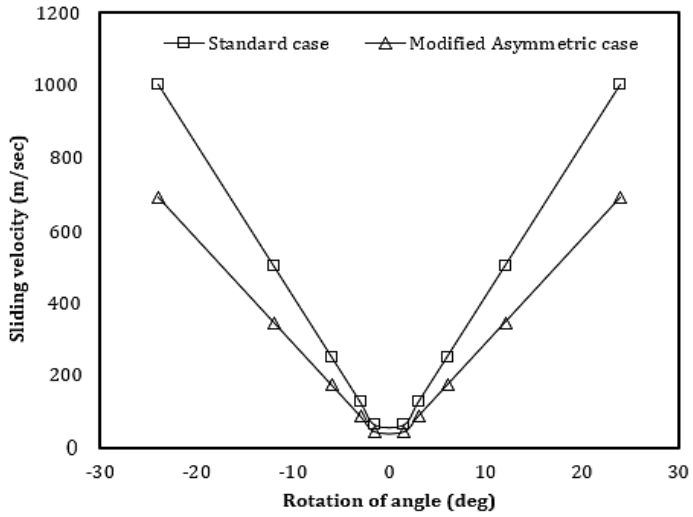

Figure 18. Comparison between the sliding velocity for two cases under different rotation of angles.

Estimating the maximum contact stress in the pitch areas and the maximum distribution stress within the teeth fillet region are also considered. All geometrical helical gears have the parameters that are shown in **Table 2**. The Von-Mises stress results were illustrated in **Fig. 19** for two cases. **Table 5** shows the values of contact stress areas and the distribution stress inside the teeth fillet region with a teeth friction coefficient value equal to 0.15. The results represented the maximum contact stress and the maximum distribution stress for both cases with the enhancement percentage compared with the standard case. It's clear that there is an enhancement in contact stress and distribution stress for the modified asymmetric helical teeth in about 12.253% and 8.91% for contact and root region, respectively. The concave-convex surface tooth profile with involute at around pitch area is supported through epicycloid and hypocycloid addition, thereby affecting the form of the global stiffness matrix for the nonparallel helical gear drive.

Table 5. The results of Von-Mises stress nonparallel helical gears.

Cases	The maximum contact stress areas σ_cMpa	Enhancement percentage	The maximum stress inside teeth fillet region σ_b Mpa	Enhancement percentage
1	250.88	-	36.943	-
2	220.140	12.253%	33.653	8.91%

According to the friction heat generation description which is represented by Eq. (17) the frictional heat fluxes magnitudes for case 1 and case 2 are about 37633.11391 W and 22742.6458 W respectively. The Enhancement percentage of improvement in heat flux

generation is about 39.567%. Normally, the temperature at the pitch point is a lower value compared to the other points such as addendum or dedendum points because the heat friction at it is relatively small due to the low sliding velocity. However, the heat conduction effect from the other parts of the tooth's body and increased the time resulting in the temperature being raised at the pitch location. The heat emitted from this region indicates the amount of friction obtained, thereby estimating the scuffing surface. The new conjugated helical teeth profile has been best with respect to the against-surface scuffing.

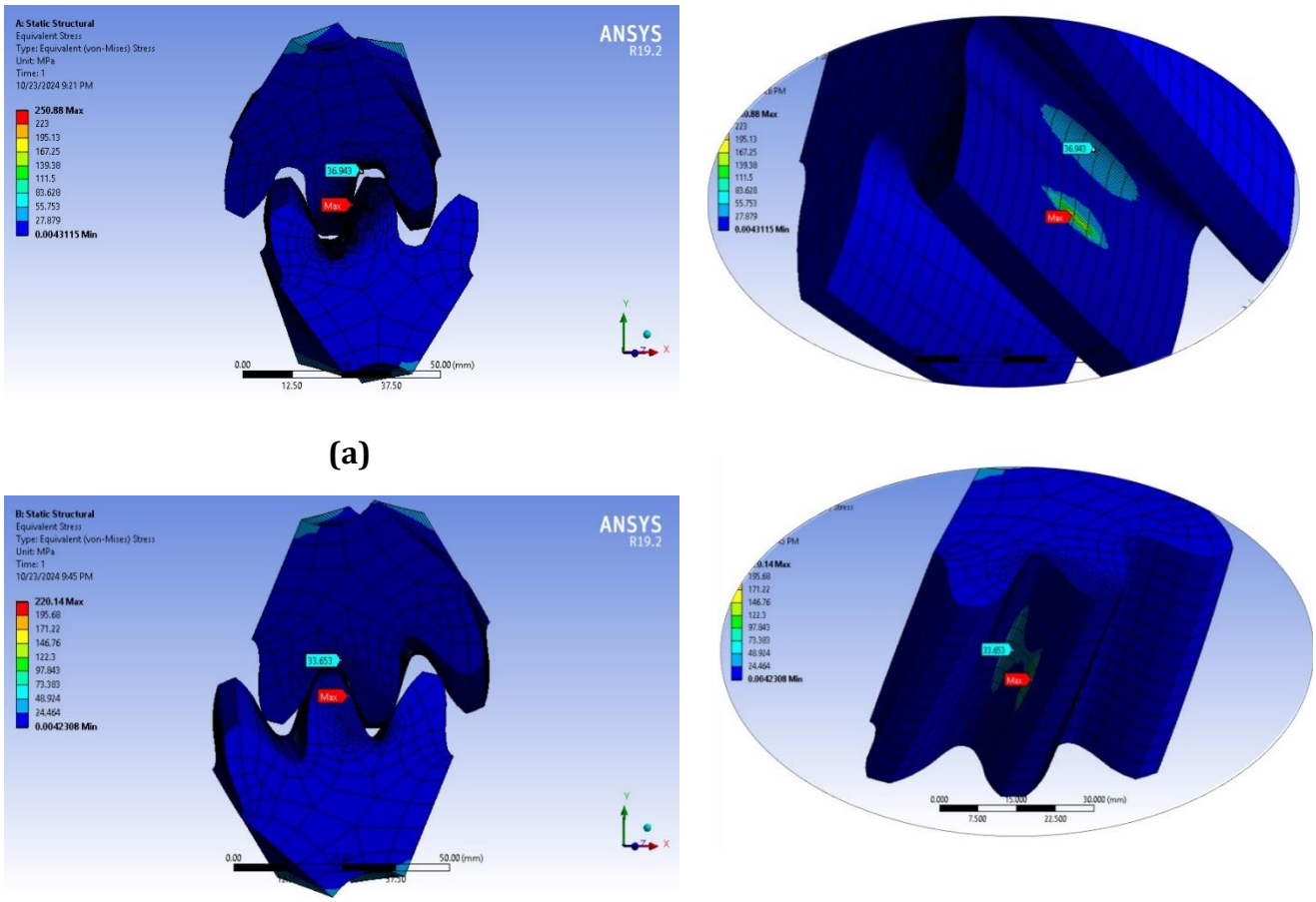

Figure 19. Von-Mises stress values for **(a)** Standard case; **(b)** Modified Asymmetric nonparallel helical gear case.

The maximum temperature distribution on the helical teeth surface for two study cases at varying rotational speeds is derived from the experimental test represented by the transient thermal analysis conducted using a thermal camera, **Figs. 20** and **21** illustrate the temperature distribution at different rotational speeds for two scenarios. It indicated that the temperature distribution is almost uniform at low speeds, but will diverge as speed increases. This study predicts heat flow using a smart thermal camera.

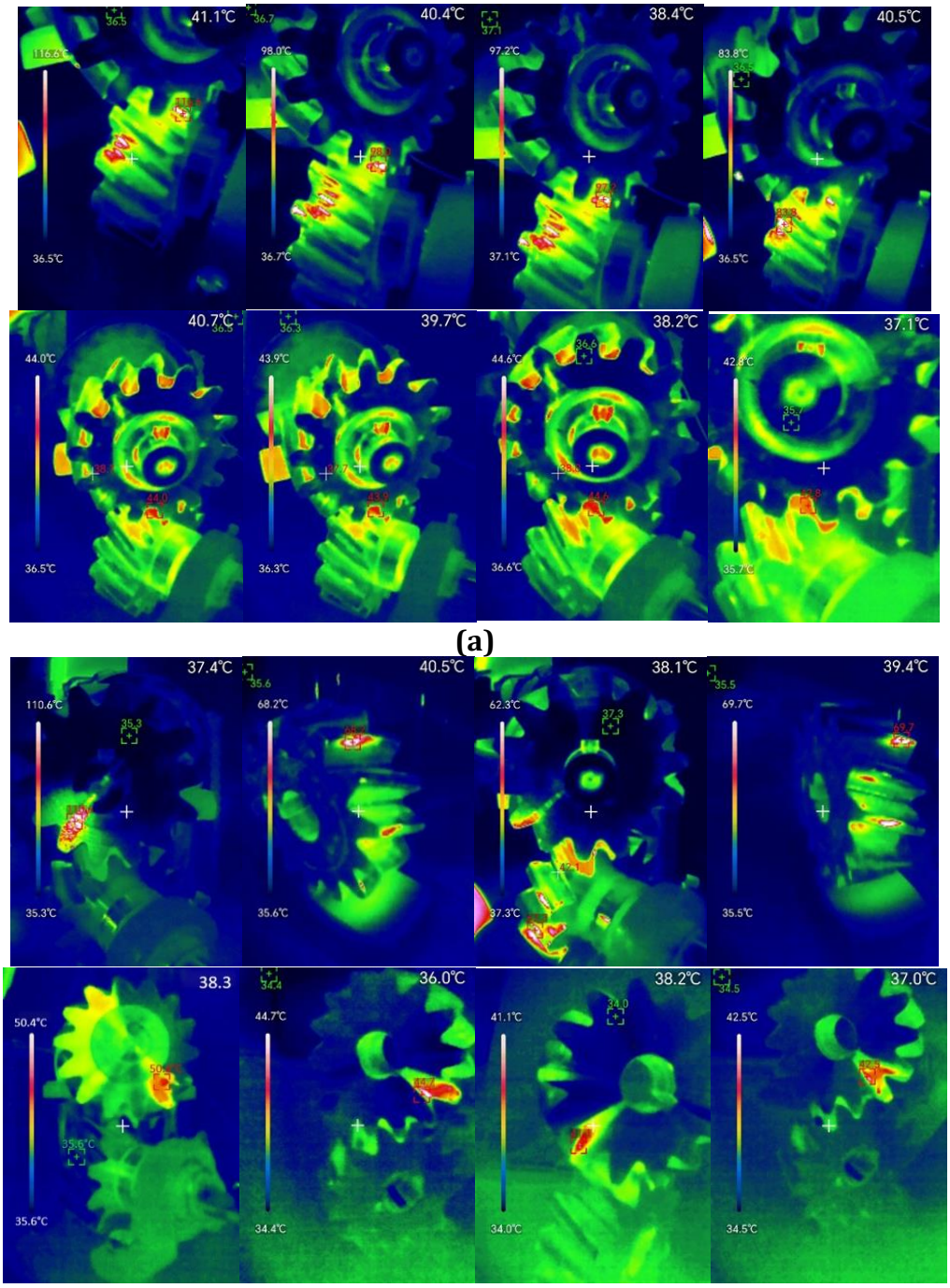

Figure 20. The temperature distribution inside; **(a)** standard non-parallel helical gear, and **(b)** Modified asymmetric non-parallel helical gear.

Due to temperature fluctuations caused by speed variations, the maximum recorded value is greatest in the standard case, attributed to the comparatively high friction between meshed teeth, which generates heat flux on the tooth surface.

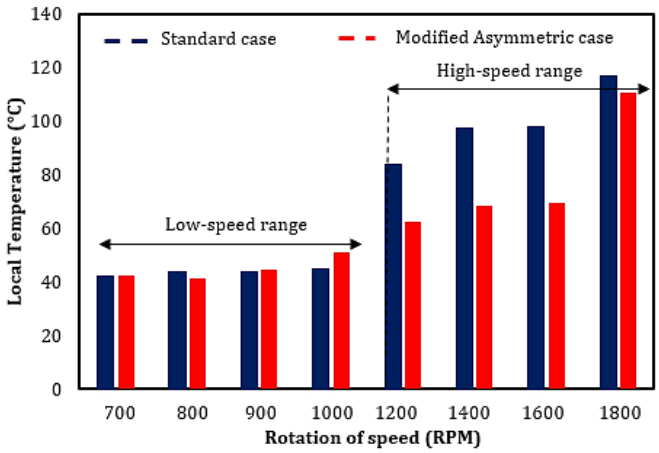

Figure 21. The temperature distribution under two ranges of speeds of rotation for two study cases.

It can be evaluated the enhancements of pitch deviation Percentage for evaluating the performance of non-parallel helical gear regarding the scuffing resistance by determining the deviations of the pitch normal at each experimental temperature value as shown in **Fig. 22** which demonstrates that the influence of tip relief, asymmetric tooth profile, and Hypocycloid flank caused an increase in the arc of contact with improved stiffness distribution inside the modified asymmetric helical teeth case. So, it can outperform the standard case about scuffing resistance.

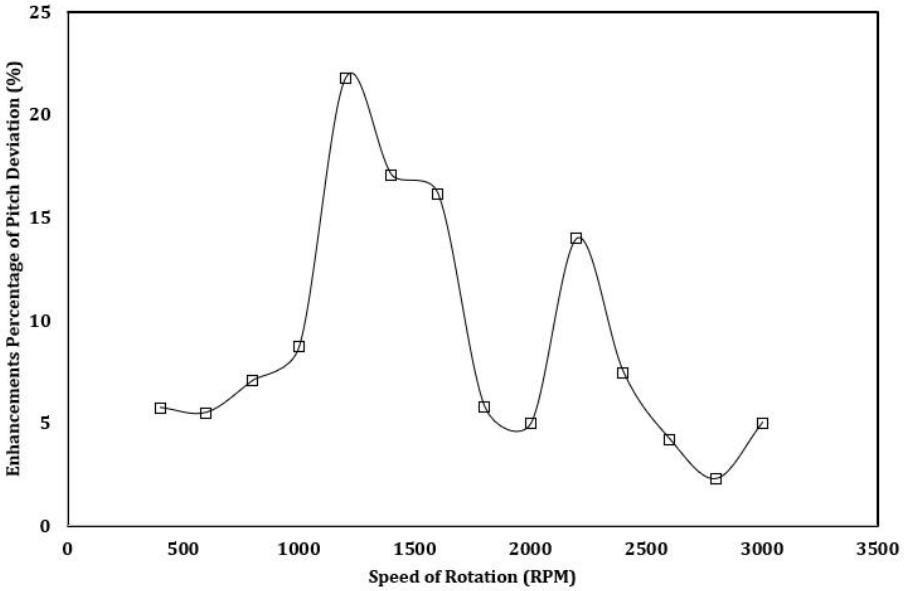

Figure 22. The enhancements of pitch deviation percentage.

6. CONCLUSIONS

The major results can be concluded from this work and summarized as follows.
The manufacturing of a new helical gear consisting of an asymmetric teeth profile with modified surface topography by creating a hybrid curve compound from three parts (hypocycloid-involute-tip relief) at the loaded side and (hypocycloid-involute-epicycloid) at the unloaded side with different pressure angles for two sides. A new special tool has been

designed for cutting the asymmetric gear tooth profiles by using the CNC machine. The numerical solution has been done by the ANSYS software package with a mesh convergence study for obtaining the maximum contact stress and tooth root stress values for two cases. The new modified asymmetric helical teeth are best as compared with the standard helical teeth of the same size, where the best enhancement percentage is about 12.253% and 8.91%. The experimental study indicates that the modification of the mated helical gears played a special role in decreasing the heat distribution inside them, which is considered a criterion for the amount of surface scuffing. Therefore, the new conjugated helical teeth profile has been best for against-surface scuffing. A smart thermal camera is a perfect tool for inspecting the thermal stability of a non-parallel helical gear drive in an approximately short period. The generated heat flux is improved by adjustment of the helical gear teeth surface; the enhancement percentage is about 39.567%. The enhancement percentage of pitch deviation under different rotational speeds has been the best compared with the standard case under the same conditions and a high-speed range with high local temperatures reaching about 15%. Despite the thermal performance of most gears being similar at low temperatures, the thermal performance of the new present non-parallel helical gear system is good in the low-speed range by 10% and then increasing.

NOMENCLATURE

Symbol	Description	Symbol	Description
α_n	Pressure angle in normal section, deg	m_n	Normal module, mm
α_t	Pressure angle in transverse section, deg	m_t	Transverse module, mm
β_p	Helix angle on the pitch cylinder, deg	z	Number of teeth
r_p	Radius of pitch circle, mm	u_r, e_r	Surface rack parameters
r_b	Radius of base circle, mm	$\vec{n}$	Surface unit normal
r_a	Radius of addendum circle, mm	ℓ	datum length for tip relief, mm
λ	Crossing angle, deg	r_ℓ	rolling length, mm
x_c, y_c	Cycloid curve dimensions	φ_ϵ	rolling angle, mm
e	correction factor	$v^{(12)}$	Sliding velocity, m/sec^2
μ	coefficient tooth friction	Q	Heat flux, W
ΔD_p	pitch deviation, mm	F_n	Tangential force, N

Acknowledgements

The authors are grateful to the crew of Central Organization for Standardization and Quality Control, Ministry of Planning Iraq—full appreciation to Al Ghabban Mechanical Industries employees. The authors thank the Mechanical Engineering Laboratory staff for their cooperation and facilitation.

Credit Authorship Contribution Statement

Mohammed Abdulaal Kadhim: Writing –original draft, Validation, Methodology. Mohammad Qasim Abdulah: Review and editing, Validation, Proofreading.

Declaration of Competing Interest

The authors declare that they have no known competing financial interests or personal relationships that could have appeared to influence the work reported in this paper.

REFERENCES

Abdulaal, M., and Abdulah, M.Q, 2024. Mathematical model and generation analysis for crossed helical gear system. *World Journal of Engineering.* https://doi.org/10.1108/WJE-01-2024-0036

Abdullah, M. Q., 2012, Analytical solution of bending stress equation for symmetric and asymmetric involute gear teeth shapes with and without profile. *Journal correction, Innovative Systems Design and Engineering, journals of IISTE.USA. 3 (6).*

Abdullah, M. Q., and Kadum, M. A., 2018. Stress concentration factor analysis of helical gear drives with asymmetric teeth profiles. *Journal of Engineering, 24, pp. 14-28.* https://doi.org/10.31026/j.eng.2018.05.02

Abdullah, M., 2003. Computer aided graphics of cycloidal gear tooth profile. In *Fifth Engineering Conference: University of Baghdad*.

Alemu, N., 2007. Analysis of Stresses in Helical Gears by Finite Element Method. PhD thesis, Department of mechanical Engineering. University of Addis Ababa, India.

Alex Kapelevich, 2009. Direct design of asymmetric gears. *In Proceedings of MPT2009-Sendai JSME International Conference on Motion and Power Transmissions May 13-15, 2009, Matsushima Isles Resort, Japan.* pp. 1-5.

Armenakas, A.E., 2005. *Advanced Mechanics of Materials and Applied Elasticity*. Boca Raton. CRC Press. ISBN: 9780429121760. 992. https://doi.org/10.1201/9781420057775

Babichev, D., 2018. Development of geometric descriptors for gears and gear tools. *Springer Nature Link,* 51, pp. 231–254. https://doi.org/10.1007/978-3-319-60399-5_11

Babichev, D., and Storchak, M., 2018. Quality characteristics of gearing. *Springer Nature Link*, 51, pp. 73–90. https://doi.org/10.1007/978-3-319-60399-5_4

Colbourne, J.R., 2012. *The geometry of involute gears*. Springer Science, Springer-Verlag New York Inc. ISBN-13: 978-1-4612-4764-7. https://doi.org/10.1007/978-1-4612-4764-7.

Farhangdoost, K., and Heirani, H., 2010. Contact stress on the surface of gear teeth with different profile. *International Journal of Mechanical and Mechatronics Engineering, 4(8), pp. 649-656.* http://doi.org/10.5281/zenodo.1085730

Gosselin, C., 2018. Multi Axis CnC Manufacturing of straight and spiral bevel gears*. Springer Nature Link,* 51, pp. 167-204. https://doi.org/10.1007/978-3-319-60399-5_8

Guilbault, R., Gosselin, C., and Cloutier, L., 2006. Helical gears, effects of tooth deviations and tooth modifications on load sharing and fillet stresses. *Journal of Mechanical Design*, 128(2), 444 https://doi.org/10.1115/1.2167650

Jelaska, D. T., 2012. *Gears and gear drives*. John Wiley and Sons Ltd, University of Split Croatia. ISBN:9781118392393. http://doi.org/10.1002/9781118392393

Juvinall, R. C., and Marshek, K. M., 2020. *Fundamentals of machine component design*. John Wiley and Sons. ISBN: 978-1-119-47568-2.

Kurowski, P., 2016. *Vibration Analysis With SolidWorks Simulation 2016.* SDC publications. ISBN-13 : 978-1630570125. 338. https://doi.org/978-1-58503-938-8

Liang D, Meng S, Tan R., 2021. Mathematical model and characteristics analysis of crossed-axis helical gear drive with small angle based on curve contact element. *Science Progress.* 104(2), pp. 1-19. https://doi.org/10.1177/00368504211016202

Linda Becker. et al., 2022. Extension of geometry and investigation of deformation on crossed helical gears to increase load capacity and performance. *International scientific journal trans and motauto world,* 7(2), pp. 42-46.

Litvin, E.L., Litvin, N.X. Chen, and Lu, j., 2007. Computerized design and generation of low-noise helical gears with modified surface topology. *Army Research Laboratory Technical Report ARL-TR-573 NASA, Technical Memorandum 106696, the University of Illinois at Chicago Chicago, Illinois,* 117(2A), pp. 254-261. https://doi.org/10.1115/1.2826131

Luo S, and Jingyu M., 2024. Manufacturing and contact characteristics analysis of a novel 2K-H internal meshing planetary reducer with involute-cycloid combined tooth profiles. *Proceedings of the Institution of Mechanical Engineers, Part C: Journal of Mechanical Engineering Science, 238(13), pp. 6706-6724*. https://doi.org/10.1177/09544062241228380

Miltenović, A., and Banić, M., 2020. Thermal analysis of a crossed helical gearbox using FEM. *Transactions of FAMENA,* 44, pp. 67-78. https://doi.org/10.21278/TOF.44106

Miltenović, A., NIkolić, V. and Banić, M., 2015. Wear load capacity of crossed helical gears with wheel made from sintered steel. *Science of Sintering, 47, pp. 153-163*. https://doi.org/10.2298/SOS1502153M

Norgauer, P., Sigmund, W., Kadach, D., and Stahl, K., 2017. Comprehensive simulation methods for crossed helical gear sets with the main focus on the calculation of contact patterns. *Forsch Ingenieurwes* 81, pp. 299–306. https://doi.org/10.1007/s10010-017-0234-0

Pakhaliuk, V., and Poliakov, A., 2018. Simulation of wear in a spherical joint with a polymeric component of the total hip replacement considering activities of daily living. *Facta Universitatis, Series: Mechanical Engineering,* 16, pp. 51-63. https://doi.org/10.22190/FUME171226006P

Pedersen N.L., 2010, Improving bending stress in spur gears using asymmetric gears and shape optimization. *Mechanism Machine Theory*, 45(11), pp. 1707-1720. https://doi.org/10.1016/j.mechmachtheory.2010.06.004

Radzevich, S. P., and Storchak, M., 2022. *Advances in gear theory and gear cutting tool design*. Springer Nature Link. ISBN 978-3-030-92262-7, 556. https://doi.org/10.1007/978-3-030-92262-7

Rattan, S. S., 2014. *Theory of machines*, Tata McGraw-Hill Education. ISBN: 978+81-920485-3-6.

Seyama, N., Nagamura, K., Ikejo, K. and Isaki, K., 2009. GSD-05 influence of design parameters on strength and driving performance of involute-cycloid composite tooth profile gears (gear strength and durability, including gear materials and heat treatment techniques). *The Proceedings of the JSME international conference on motion and power transmissions*. *The Japan Society of Mechanical Engineers*, pp. 329-332. https://doi.org/10.1299/jsmeimpt.2009.329

Smith, J. D., 2003. *Gear noise and vibration*, 270 Madison Avenue, New York, NY 10016. ISBN: 0-8247-4129-3.

Stolarski, T., Nakasone, Y., and Yoshimoto, S., 2018. *Engineering analysis with ANSYS software*. Elsevier Ltd. ISBN-978-0-08-102164-4.

Temirkhan, M., Tariq, H. B., Kaloudis, K., Kalligeros, C., Spitas, V., and Spitas, C., 2022. Parametric Quasi-Static Study of the Effect of Misalignments on the Path of Contact, Transmission Error, and Contact Pressure of Crowned Spur and Helical Gear Teeth Using a Novel Rapidly Convergent Method. *Applied Sciences, 12(19), 10067*. https://doi.org/10.3390/app121910067

Trubachev, E., Savelyeva, T., and Pushkareva, T., 2018. *Practice of Design and Production of Worm Gears with Localized Contact*. Springer *International Publishing Switzerland,* pp. 327-343. https://doi.org/10.1007/978-3-319-60399-5_16

Vijayaraghavan, G., and Vishnupriyan, S., 2009. *Design of Machine Elements*. Lakshmi. ISBN-978-81-920485-3-6.

Wang, Y., Liu, Y., Tang, W., and Liu, P. 2017. Parametric finite element modeling and tooth contact analysis of spur and helical gears including profile and lead modifications. *Engineering Computations*, 34(8), pp. 2877-2898. https://doi.org/10.1108/EC-06-2016-0203

Wang, Y., Tang, W., Chen, Y., Wang, T., Li, G. and Ball, A. D., 2017. Investigation into the meshing friction heat generation and transient thermal characteristics of spiral bevel gears. *Applied Thermal Engineering*, 119, pp. 245-253. https://doi.org/10.1016/j.applthermaleng.2017.03.071.

Wu, J., Wei, P., Zhu, C. et al., 2024. Development and application of high strength gears. The *International Journal of Advanced Manufacturing Technology*, 132, pp. 3123–3148. https://doi.org/10.1007/s00170-024-13479-x

Yazdani M., Soteriou M.C., Sun F., and Chaudhry Z., 2015. Prediction of the thermo-fluids of gearbox systems. *International Journal of Heat and Mass Transfer*, 81, pp. 337-346. https://doi.org/10.1016/j.ijheatmasstransfer.2014.10.038

تحسين أداء محرك التروس الحلزوني غير المتوازي باستخدام الأسنان غير المتماثلة المعدلة مع تشذيب الحواف

محمد عبد العال كاظم*، محمد قاسم عبد الله

قسم الهندسة الميكانيكية، كلية الهندسة، جامعة بغداد، بغداد، العراق

الخلاصة

ارتفاع درجة الحرارة هو المشكلة العامة لنظام التروس الحلزوني غير المتوازي. والسبب هو الاحتكاك العالي وسرعة الانزلاق والقوة العرضية التي تحدث بين أسنان التروس المتشابكة. هذه تؤدي إلى عواقب سيئة مثل زيادة فقدان الطاقة ، وانخفاض كفاءة التروس ، والانهيار ، والجرجرة. تم استخدام نوعين من التروس الحلزونية غير المتوازية لتقدير تدفقات الحرارة المتشابكة لزوج من أنظمة التروس غير المتوازية. الحالة القياسية مع نظام حلزوني غير متوازي غير متماثل معدل. تم تصميم أداة خاصة جديدة لقطع تضاريس السطح المعدلة لمحات أسنان التروس غير المتماثلة. هذه الأداة غير متماثلة ويمكن اعتبارها مرجعا لإعداد معدات حلزونية غير متماثلة معدلة مماثلة للقاطع بواسطة آلة التصنيع باستخدام الحاسب الآلي. تصنيع ترس حلزوني جديد يتكون من شكل أسنان غير متماثل مع تضاريس سطحية معدلة عن طريق إنشاء مركب منحنى هجين من ثلاثة أجزاء (تشذيب الحواف ناقص الحلقي–مطوي) في الجانب المحمل و (ناقص الحلقي–مطوي–حلقي) في الجانب غير المحمل بزوايا ضغط مختلفة للجانبين. محرك التروس الحلزوني غير متوازي الذي تم تعديل أسنانه بشكل غير متماثل أفضل من محرك التروس الحلزوني القياسي غير المتوازي. أفضل التحسينات للحد الأقصى للإجهاد التلامسي ونسبة إجهاد جذر الأسنان هي حوالي 12.253 ٪ و 8.91٪. تم تحسين تدفق الحرارة المتولد عن طريق تعديل سطح أسنان التروس الحلزونية ، ونسبة التحسين حوالي 39.567٪. كانت نسبة التحسين لانحراف الملعب تحت سرعات دوران مختلفة هي الأفضل مقارنة بمحرك التروس القياسية في نفس الظروف ونطاق عالي السرعة مع درجات حرارة محلية عالية تصل إلى حوالي 15 ٪ وهي جيدة اما في نطاق السرعة المنخفضة تصل النسبة 10٪.

الكلمات المفتاحية: الأسنان الحلزونية غير المتماثلة المعدلة، تعديل تشذيب الحواف، معامل احتكاك الأسنان، إجهاد التلامس، الاحتكاك الحراري المتولد.